AGU PUBLICATIONS

JGR

Journal of Geophysical Research: Atmospheres

RESEARCH ARTICLE

10.1002/2014JD022361

Modeling the impact of snow drift on the decameter-scale variability of snow properties on the Antarctic Plateau

Quentin Libois[1,2], Ghislain Picard[1,2], Laurent Arnaud[1,2], Samuel Morin[3], and Eric Brun[4]

[1]University of Grenoble Alpes, LGGE (UMR5183), F-38041 Grenoble, France, [2]CNRS, LGGE (UMR5183), F-38041 Grenoble, France, [3]Météo-France – CNRS, CNRM – GAME UMR 3589, Centre d'Etudes de la Neige, Grenoble, France, [4]Météo-France – CNRS, CNRM – GAME UMR 3589, GMGEC, Toulouse, France

Key Points:
- Drift is simulated with Crocus to explain the variability of snow properties
- The observed vertical profiles of SSA and density at Dome C are well reproduced
- Spatial variability in accumulation at Dome C is due to snow drift

Correspondence to:
Q. Libois,
quentin.libois@lgge.obs.ujf-grenoble.fr

Citation:
Libois, Q., G. Picard, L. Arnaud, S. Morin, and E. Brun (2014), Modeling the impact of snow drift on the decameter-scale variability of snow properties on the Antarctic Plateau, *J. Geophys. Res. Atmos.*, *119*, 11,662–11,681, doi:10.1002/2014JD022361.

Received 28 JUL 2014
Accepted 2 OCT 2014
Accepted article online 5 OCT 2014
Published online 29 OCT 2014

Abstract The annual accumulation and the physical properties of snow close to the surface on the Antarctic Plateau are characterized by a large decameter-scale variability resulting from snow drift that is not simulated by one-dimensional snow evolution models. Here, the detailed snowpack model Crocus was adapted to Antarctic conditions and then modified to account for this drift-induced variability using a stochastic snow redistribution scheme. For this, 50 simulations were run in parallel and were allowed to exchange snow mass according to rules driven by wind speed. These simple rules were developed and calibrated based on in situ pictures of the snow surface recorded for two years. The simulation performed with this new model shows three substantial improvements with respect to standard Crocus simulations. First, significant and rapid variations of snow height observed in hourly measurements are well reproduced, highlighting the crucial role of snow drift in snow accumulation. Second, the statistics of annual accumulation is also simulated successfully, including the years with net ablation which are as frequent as 15% in the observations and 11% in the simulation. Last, the simulated vertical profiles of snow density and specific surface area down to 50 cm depth were compared to 98 profiles measured at Dome C during the summer 2012–2013. The observed spatial variability is partly reproduced by the new model, especially close to the surface. The erosion/deposition processes explain why layers with density lower than 250 kg m^{-3} or specific surface area larger than 30 m^2 kg^{-1} can be found deeper than 10 cm.

1. Introduction

The physical properties of surface snow influence the energy balance of the Antarctic ice sheet [*van de Berg et al.*, 2006; *Brun et al.*, 2011]. They determine snow albedo [*Scambos et al.*, 2007], whose slight changes can have a large impact on the Antarctic climate [*Hansen*, 2004; *Picard et al.*, 2012]. They also alter the exchanges of heat, water vapor, and momentum with the atmosphere through the surface roughness [*King and Anderson*, 1994]. In addition, snow properties impact the mass balance of the ice sheet because snow drift, which is responsible for snow sublimation and redistribution, depends on the cohesiveness of the surface [*Lenaerts et al.*, 2012; *Das et al.*, 2013]. Accurately modeling snow properties is thus essential to estimate the contribution of Antarctica to sea-level rise [*Shepherd and Wingham*, 2007; *Eisen et al.*, 2008]. However, a specificity of the Antarctic Plateau, a large area characterized by high elevation (>2500 m) and low annual accumulation [*Arthern et al.*, 2006], is that the physical processes which influence snow characteristics there are not yet fully understood compared to other regions where accumulation is much larger [e.g., *Frezzotti et al.*, 2005; *Kameda et al.*, 2008]. Understanding these processes is necessary to model climate feedbacks involving snow-atmosphere interactions [*Hall*, 2004] and to perform climate projections in a context of global warming [e.g., *Krinner et al.*, 2007]. It is also of interest for paleoclimatological applications. For instance, *Raynaud et al.* [2007] and *Hutterli et al.* [2009] have investigated the correlation between the volume of air contained in ice cores and local insolation, showing that surface processes can determine the properties of firn and ice at depth [*Albert et al.*, 2004; *Fujita et al.*, 2009]. The interpretation of isotopic signals also requires a quantitative understanding of the interactions between the snowpack and the atmosphere [*Fujita and Abe*, 2006; *Steen-Larsen et al.*, 2011]. Moreover, the physical properties of snow impact its radiative properties, a critical point for the interpretation of remote sensing data on the Antarctic Plateau [e.g., *Jin et al.*, 2008; *Lacroix et al.*, 2009].

Snow properties on the Antarctic Plateau exhibit a high decameter-scale horizontal variability [e.g., *Gallet et al.*, 2011; *Picard et al.*, 2014]. Accumulation is also highly variable in space [*Petit et al.*, 1982; *Palais et al.*,

1983] and time [*Frezzotti et al.*, 2005], even considering annual and multidecadal averages. This variability is not only due to atmospheric variability but also results from the combined effects of snow transport by the wind [*Goodwin*, 1990] and post-depositional processes operating before snow is definitively buried [*Albert et al.*, 2004; *Courville et al.*, 2007]. The role of wind has long been pointed out [*Koerner*, 1971; *Kuhn et al.*, 1977]. It constantly forms sastrugi whose height often exceeds the average annual accumulation [*Gow*, 1965] and alters greatly snow properties [*Sugiyama et al.*, 2012; *Scambos et al.*, 2012]. Drift events also redistribute snow through erosion and deposition processes at meter to kilometer scale [*Gallée et al.*, 2001; *Lenaerts et al.*, 2012], which generates spatial variability in accumulation.

One consequence of snow drift is that snow stratification at Dome C barely reflects a clear history of the snowpack as it is common in alpine environments for instance, and snow profiles measured a few meters of each other can show very different stratifications. Snow redistribution by the wind thus introduces white noise that alters ice core reconstructions [*Fisher et al.*, 1985], making it difficult to accurately date ice cores at yearly resolution [*Kameda et al.*, 2008]. In particular, the alternation of coarse faceted crystals with wind packed layers common in Greenland, which allows counting of the individual layers up to 60,000 years at some sites [*Alley*, 1988; *Svensson et al.*, 2008], is not clearly visible on the Antarctic Plateau [*Petit et al.*, 1982; *Fujita et al.*, 2009]. Since the residence time of snow close to the surface depends on the accumulation rate, the latter influences snow metamorphism [*Dang et al.*, 1997; *Hutterli et al.*, 2009]. Indeed, snow that remains at the surface experiences large and varying temperature gradients [*Colbeck*, 1989] which sustain intense water vapor transport and result in strong grain growth and other morphological changes [*Sturm and Benson*, 1997; *Albert et al.*, 2004] while snow that is rapidly buried is exposed to much lower temperature gradients and ventilation [*Albert*, 2002], yielding smaller grains.

The objective of the paper is to simulate the spatial decameter-scale variability of snow properties with a multilayer detailed snowpack model. Only a few studies report simulations performed with such models on the Antarctic Plateau. *Dang et al.* [1997] already ran Crocus [*Brun et al.*, 1989] at South Pole and compared simulated profiles of density and visual grain size to in situ profiles. In this case, Crocus was forced with atmospheric analyses from the European Centre for Medium-Range Weather Forecasts (ECMWF) and adapted to polar conditions by defining a wind-dependent density for fresh snow consistent with observed surface density. To improve the representation of snow cover in climate simulations, *Brun et al.* [1997] coupled Crocus to a global circulation model and implemented post-depositional compaction of surface snow by the wind to fit temperature profiles at South Pole. More recently, the ability of Crocus to reproduce the surface energy balance at Dome C was highlighted by comparing a 10 day simulation forced by local meteorological observations to observed temperature profiles [*Brun et al.*, 2011]. However, the length of the simulation did not allow to evaluate snow metamorphism. Using a 13 year simulation, *Fréville et al.* [2014] showed that Crocus forced by ECMWF ERA-Interim reanalysis [*Dee et al.*, 2011] could simulate successfully the snow surface temperature over a large area of Antarctica. *Groot Zwaaftink et al.* [2013] investigated the impact of drift events on snow accumulation at Dome C, by comparing observed evolution of snow height to SNOWPACK [*Lehning et al.*, 2002] simulations forced with meteorological observations. This model was adapted to the Antarctic Plateau environment, in particular by using an empirical wind-dependent density for fresh snow to account for the effect of snow compaction by the wind.

All these simulations, which assume a gradual accumulation of precipitation, proved sufficient to model the energy budget of the snowpack but did not reproduce the observed vertical variability of density and visual grain size. *Dang et al.* [1997] investigated the sensitivity of the simulated snow properties to precipitation amount, a quantity that can hardly be measured or predicted accurately on the Antarctic Plateau [*Bromwich et al.*, 2011]. To this end, they simulated accumulation variability by adding white noise to the precipitation input, which produced vertical variability in the simulations, but not horizontal variability. Another step forward was made by *Groot Zwaaftink et al.* [2013], who reported that snow height variations at Dome C were often decorrelated from observed precipitation events. To account for this in SNOWPACK, they considered that snow was deposited only during wind events, which they defined as periods of 100 h with average wind speed larger than 4 m s^{-1} (measured at 3 m height). Although this representation is limited because in reality snow is deposited before to be drifted, they showed that it improved the agreement between observed and simulated snow heights. They also compared simulated profiles of density and grain size to measurements and highlighted the difficulty to compare simulations with observations due to the high spatial variability of snow properties. They pointed out that their model did not account explicitly for erosion and deposition at the surface, while such subgrid processes were frequent at Dome C. For instance, only

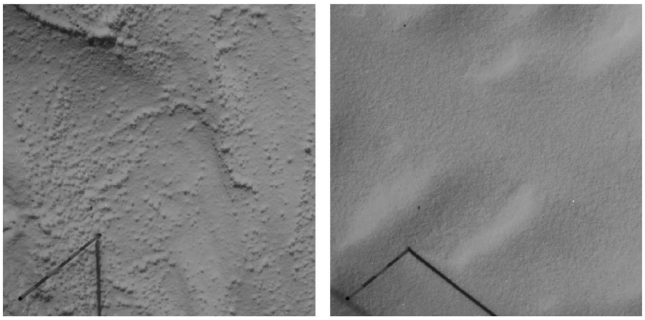

Figure 1. These two pictures, taken at a 2 h interval, show a 0.5 m × 0.5 m snow surface area before and during a drift event on 19 December 2011 and exhibit a 10 cm variation of snow height (the dark and clear bands on the stake are 5 cm long).

snow transport can explain the years with net ablation reported by *Petit et al.* [1982] at Dome C, because sublimation is much lower than mean annual accumulation at Dome C [*Frezzotti et al.*, 2004]. In short, the observed spatial variability of snow properties is not accounted for by models based on one-dimensional concepts such as plan-parallel layers and uniform meteorological forcing.

In this paper, snow erosion and redistribution by the wind are modeled with Crocus in order to simulate the variability of annual accumulation and profiles of snow properties, with potential applications for studies dedicated to mass balance and snow physical properties. To this end, we represent snow transport with a simple statistical approach since an explicit and physically based representation of snow transfers at the decameter-scale is virtually impossible at this time. Indeed, most simulations of snow transport in alpine terrain are performed at the scale of a few tens of meters [*Lehning and Fierz*, 2008; *Vionnet et al.*, 2014], and higher resolution simulations are computationally very expensive [*Liston et al.*, 2007; *Mott and Lehning*, 2010]. The statistical representation is built upon a detailed analysis of drift events conducted from observations of snow height variations at Dome C. This parameterization is evaluated in the light of field observations of point scale annual accumulation and snow properties. To this end, a large number of density and specific surface area (the surface area of the ice-air interface per unit mass of snow, hereafter referred as SSA) measurements taken at high vertical and temporal resolution during the austral summer 2012–2013 is used. This gives for the first time a statistically representative sample of these two essential physical properties of snow [*Domine et al.*, 2008] at Dome C.

2. Field Observations

The measurements used in this study combine automatic and manual measurements of snow height, snow density, and snow SSA, taken at Dome C close to Concordia station (75.1°S, 123.3°E, 3230 m above sea level).

2.1. Snow Height Measurements

2.1.1. Hourly Snow Height Variations

Snow height was measured at high temporal resolution in one point located about 600 m West of Concordia station. A camera (Canon EOS 5D) packaged in a heated box took automatically hourly pictures of a 2 m × 2 m snow surface area with a graduated metallic stake 50 cm long in the frame (Figure 1), from 10 January 2011 to 20 February 2013, with interruption due to the failure of the system not exceeding 10% of the time [*Champollion et al.*, 2013]. Pictures are available even during the polar night by using spot lights. Snow height at one point could thus be estimated at ±0.5 cm through visual inspection. We checked in the pictures that the presence of the stake did not perturb the snow surface. The time series of snow height is shown in Figure 2a. Daily variations are sometimes large, even larger than the annual accumulation on some occasions (e.g., on 23 February 2011). A detailed analysis of the pictures showed that these large variations often corresponded to the formation or displacement of local relief such as dunes and sastrugi [*Gow*, 1965]. Figure 3 shows an example of such formation of typical height 10 cm, formed in a few hours. These snow height variations cannot be explained solely by precipitation and are essentially due to snow deposition and transport occurring during strong wind events.

The statistics of drift events was deduced from these observations of snow height and used further to build the stochastic representation of erosion and deposition. In this study, we considered as "drift events" the variations of snow height larger than 1 cm which occurred in less than 24 h. Such variations could hardly be due to precipitation alone because daily precipitation in ERA-Interim reanalysis was always lower than 1.5 kg m^{-2} (or approximately 1 cm assuming the density of fresh snow is about 150 kg m^{-3}) at Dome C during the period of observation (except for one event on 13 June 2012). Although ERA-Interim reanalysis tends to underestimate precipitation on the East Antarctic Plateau [*Bromwich et al.*, 2011], precipitation events

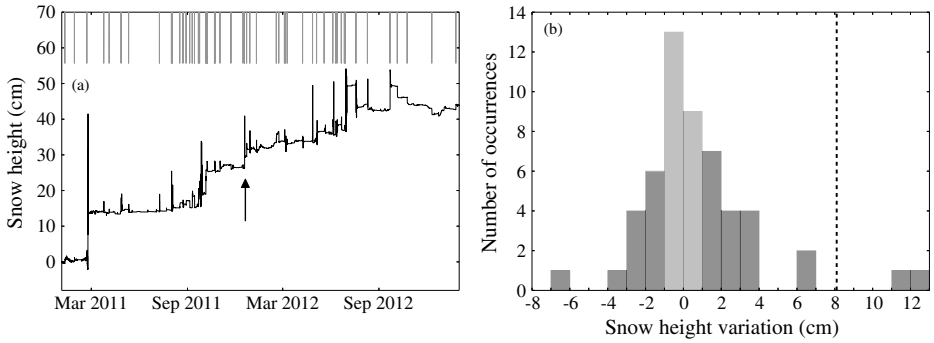

Figure 2. (a) Hourly time series of snow height obtained from pictures of the snow surface. Vertical bars at the top highlight when drift events were detected from the snow height variations. The vertical arrow points to the drift event illustrated in Figure 1. (b) Distribution of snow height variations during the 53 drift events identified from pictures of the snow surface. The vertical dashed line indicates the mean annual accumulation from GLACIOCLIM stake network.

larger than 1 cm of snow (which represents 10% of the mean annual accumulation) are rarely observed at Dome C. Based on snow height variations at the stake, 53 events were thus identified during the period (Figure 2a). For each drift event, the difference between snow height at the end and at the beginning of the event was computed, and the distribution of snow height variations is presented in Figure 2b. Twelve events correspond to net erosion larger than 1 cm and 19 to net accumulation larger than 1 cm. The 22 events with net variations less than 1 cm often corresponded to the passage of some relief through the field of view of the camera which essentially left the surface unaltered at the end of the event. Here, only accumulation larger than 1 cm was considered as genuine deposition.

In addition to stake height, snow movements were identified from the analysis of the whole pictures. These movements indicate that drift is occurring, even though it may not result in detectable variation of snow height at the stake. During the investigated period, 101 drift events were thus identified, including the 53 events with snow height variations reported before. According to Figure 2b, in 19 cases out of 101, these drift events resulted in snow deposition at the stake. Under the ergodic hypothesis, we conclude that at each drift event, significant amounts of snow are deposited over approximately 20% of the total area only.

2.1.2. Annual Snow Height Variations

Annual snow height variations are measured on 50 stakes 2.5 m long installed by the GLACIOCLIM-SAMBA (SurfAce Mass Balance of Antarctica, http://www-lgge.obs.ujf-grenoble.fr/ServiceObs/index.htm) observatory [e.g., *Eisen et al.*, 2008]. The stakes are arranged in a 1 km × 1 km cross located 3 km South of Concordia station, with approximately 50 m between neighboring stakes. Their emergence, initially 1.6 m, was measured several times a year from 2004 to 2012. As we focused on the statistics of annual variations of snow height, only one measurement per year was selected, that closest to December 1st. This resulted in a set of 400 annual height variations, whose distribution is shown in Figure 4. The mean annual variation is 8.1 cm, and the standard deviation is 8.8 cm. This corresponds to 28±31 kg m^{-2} a^{-1} using the method of *Takahashi and Kameda* [2007] and assuming a density of 350 kg m^{-3} at the base of the stakes. This value agrees with

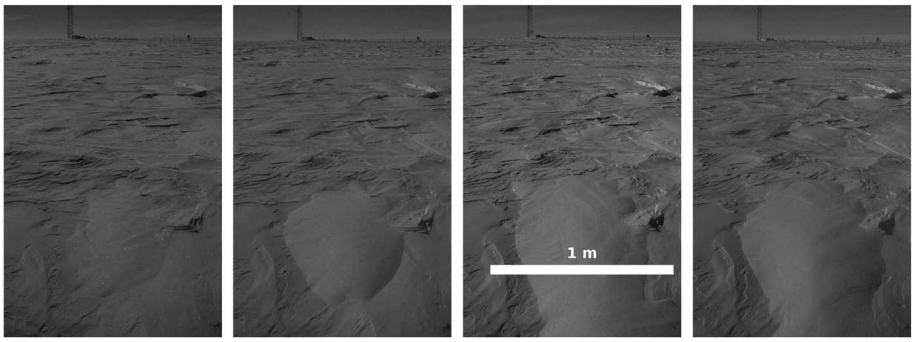

Figure 3. A series of four pictures of the snow surface taken at a 1 h interval close to Concordia station on 29 November 2013, showing the formation of a thick snow patch whose thickness and horizontal extent are approximately 10 cm and 1 m^2.

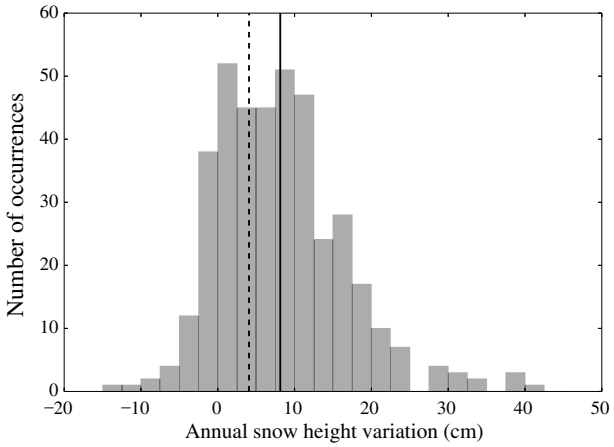

Figure 4. Distribution of the 400 annual snow height variations measured on the network of 50 stakes from 2004 to 2012. The vertical continuous line indicates the mean height variation and the dashed line indicates half the mean variation.

the annual accumulation determined by *Frezzotti et al.* [2004] from Tritium/β level markers close to Dome C: 28.3 kg m^{-2} a^{-1}. Considering individual stakes, the annual accumulation ranges from approximately −50 to 130 kg m^{-2} a^{-1}. Since the mean annual snow height variation does not show any significant trend during the investigated period, the observed variability is essentially due to spatial variability of accumulation. Out of the 400 values of annual accumulation, 60 are negative, which means that net ablation from one year to another occurs as much as 15% of the time. Moreover, 82 values (21%) are lower than half the average accumulation. These statistics compare well with those reported by *Petit et al.* [1982] at Dome C and by *Kameda et al.* [2008] at Dome Fuji. The 8 year height variations were also calculated for the 50 stakes. Their standard deviation, 10.8 cm, is similar to the 1 year variability, highlighting that snow transport tends to level out the snow surface on the long term [*Kameda et al.*, 2008].

2.2. Vertical Profiles of Density and SSA

During the summer campaign 2012–2013, 98 collocated profiles of density and SSA were measured from 23 November 2012 to 16 January 2013 at two different sites. The first site is 600 m West of the main building of Concordia station and the second site is 500 m South East of the station. Every day during this period (except from 3 to 6 January), two profiles of density and SSA were measured, one day at the first site, the other day at the other site. All these profiles were separated by at least 5 m from each other. Vertical profiles of density were measured from the surface to 25 cm depth, at 2.5 cm vertical resolution. For this, a rectangular cutter of dimensions $2.5 \times 10 \times 10$ cm was used. Vertical profiles of SSA at 1 cm vertical resolution were taken with the profiler ASSSAP (a light version of POSSSUM) [*Arnaud et al.*, 2011], from the surface to approximately 50 cm, depending on the ability of the snow cutter to perforate hard wind packed layers. ASSSAP measures vertical profiles of reflectance at 1310 and 805 nm, from which the SSA is deduced using a complex algorithm [*Arnaud et al.*, 2011].

3. Crocus Simulations

The detailed snowpack model Crocus was used to simulate snow properties at Dome C. After introducing the general features of Crocus, the various simulations performed are presented. The simulation 1D-Std uses the standard version of Crocus. The simulations 1D-Ant and 1D-Ant' use a version adapted to the meteorological conditions of Dome C. The simulations MP, MP', and MP" are based on the multipatch version presented here where snow can be eroded and transported from a patch to another. The characteristics of all the simulations are summarized in Table 1 and detailed in the following sections.

3.1. Description of Crocus and Meteorological Forcing

SURFEX/ISBA-Crocus [*Vionnet et al.*, 2012] simulates the evolution of the physical properties of a one-dimensional multilayer snowpack given initial conditions and atmospheric forcing. It accounts for several physical processes among which: precipitation deposition, snow metamorphism, post-depositional compaction of surface snow by the wind, snow settlement, and surface energy budget. The prognostic variables for snow layers relevant for this study are layer thickness, snow density, snow temperature, snow SSA, and snow sphericity [*Carmagnola et al.*, 2014]. As detailed in *Carmagnola et al.* [2014], three options are available for snow metamorphism in the case where SSA and sphericity are the main prognostic variables describing snow microstructure: the reformulation of the original parameterization of *Brun et al.* [1992] (called hereinafter C13), the semiempirical parameterization of *Flanner and Zender* [2006] (called F06), and the parameterization based on the measurements of *Taillandier et al.* [2007] (called T07). The latter is not

Table 1. Crocus Simulations Used in This Study[a]

Simulation	Characteristics
1D-Std	Standard version
1D-Ant	Version adapted to Dome C conditions
1D-Ant′	Same as 1D-Ant, precipitation deposited after drift events as defined by *Groot Zwaaftink et al.* [2013]
MP	Multipatch version
MP′	Same as MP, SSA of drifted snow increased by 10 m^2 kg^{-1}
MP″	Same as MP, rate of growth of optical radius divided by two

[a]The details about simulations 1D-Ant and MP are given in sections 3.2 and 3.3.

suited for snow on ice sheets, as pointed out by *Carmagnola et al.* [2014], and is not used in this study. The parameterization F06 is formulated in terms of optical radius increase [*Oleson et al.*, 2010]. The effect of snow drift is taken into account through post-depositional compaction by the wind that increases the density of the topmost layers of the snowpack if their driftability index S_l is positive. This index, which describes the potential for snow erosion in given wind conditions, is given by

$$S_l = -2.868 \exp\left(-0.085 u_5\right) + 1 + M_O, \quad (1)$$

where u_5 is the wind speed at 5 m and the mobility index, M_O, depends on snow density, snow sphericity and snow SSA [*Guyomarc'h and Mérindol*, 1998; *Gallée et al.*, 2001; *Vionnet et al.*, 2012; *Carmagnola et al.*, 2014].

Crocus handles a maximum of 50 numerical layers in the present study. When precipitation occurs while the snowpack already comprises 50 layers, some internal layers are aggregated to allow a new layer to form at the surface. More generally, the aggregation scheme of Crocus automatically handles the numerical layers to account for the natural stratification of the snowpack imposed by precipitation while maintaining an accurate calculation of the temperature profile. The layers thickness dynamically evolves over time due to densification. In addition, adjacent layers can be aggregated, according to the similitude of their physical properties. A thick layer can also be split to refine the resolution of the temperature profile. The model also attempts to conform to a user-defined optimum vertical grid which minimizes layer thickness near the top of the snowpack to better describe subsurface processes such as solar radiation penetration and heat diffusion.

For the simulations performed at Dome C, atmospheric forcings were obtained from the 3-hourly ERA-Interim 2 m air temperature and specific humidity, surface pressure, precipitation amount, wind speed at 10 m, and downward radiative fluxes. The average amount of ERA-Interim precipitation during the period is 19.8 kg m^{-2} a^{-1}, which is approximately 35% lower than the average accumulation of 29 kg m^{-2} a^{-1} reported by *Frezzotti et al.* [2004] and GLACIOCLIM-SAMBA data. We thus multiplied the precipitation by 1.5, which resulted in accumulation similar to the observations because net simulated sublimation was less than 1 kg m^{-2} a^{-1}. This simple multiplication is based on the observation that ERA-Interim captures relatively well precipitation occurrence [*Palerme et al.*, 2014] but fails at reproducing the measured annual accumulation on the Antarctic Plateau [*Bromwich et al.*, 2011]. The atmospheric forcing from 2000 to 2010 was used 3 times consecutively after the snowpack was initialized down to 12 m with density, SSA, and temperature measurements performed at Dome C [*Picard et al.*, 2014], to correctly resolve the temperature gradients. This ensured that the top 2 m at the end of this spin-up were composed of accumulated snow. The model was then run from 2000 to 2013.

3.2. Simulations Adapted to Dome C Conditions (1D-Ant and 1D-Ant′)

The simulation 1D-Std was obtained with the standard version of Crocus. However, running a detailed snowpack model in a polar environment requires specific modifications compared to alpine simulations [*Dang et al.*, 1997; *Groot Zwaaftink et al.*, 2013]. For simulation 1D-Ant, the properties of fresh snow, the parameterization of post-depositional snow compaction by the wind, and the aggregation scheme were thus adapted as follows.

The original parameterization of fresh snow density based on temperature and wind invariably leads to a density of 50 kg m^{-3}, which is lower than any of the reported observations of surface snow density at Dome C. *Dang et al.* [1997] modified this parameterization to obtain surface snow density similar to observations. Likewise, *Groot Zwaaftink et al.* [2013] suggested a parameterization of fresh snow density depending on wind speed to fit their density measurements. These parameterizations led to densities larger than

250 kg m^{-3} because they implicitly included post-depositional compaction by the wind, a process that was not modeled. Because this process is now included in Crocus, we chose to set the density of fresh snow to 170 kg m^{-3}, which corresponds to the fifth lowest percentile of the measured surface densities at Dome C during the 2012–2013 campaign. This choice was based on the assumption that snow with lowest density had barely been altered by post-depositional processes.

The SSA of fresh snow was set to 100 m^2 kg^{-1}, a value representative of our measurements of precipitating snow and diamond dust collected during precipitation events. This is more than the maximum SSA of fresh snow in the standard version of Crocus, 65 m^2 kg^{-1}, but close to 110 m^2 kg^{-1}, corresponding to an optical radius of 30 μm mentioned by *Grenfell et al.* [1994] for the surface snow layers at South Pole and Vostok. This is less than the 140 m^2 kg^{-1} and 270 m^2 kg^{-1} estimated by *Walden et al.* [2003] for, respectively, snow and diamond dust in winter at South Pole.

In the standard version of Crocus, the maximum snow density in near surface snow which can be attained through wind-induced densification is 350 kg m^{-3}. Higher values due to compaction by the wind are not considered. *Brun et al.* [1997, 2013] have shown that this parameterization could lead to a negative bias of simulated density. Here, we increased this value to 450 kg m^{-3} to account for observation of snow density on the Antarctic Plateau larger than 350 kg m^{-3} [e.g., *Albert et al.*, 2004].

The aggregation scheme for numerical layers was adapted to handle the low amounts of precipitation encountered at Dome C. The user-defined profile of layers thickness was modified so that the topmost 10 layers are thinner than in the standard version (the 5 topmost layers of this new profile are 2, 3, 5, 5, and 10 mm thick respectively). The minimum rate of precipitation which can form new layers was decreased by a factor 10 (down to 0.003 mm h^{-1}) and aggregation was deactivated for the top eight layers. ERA-Interim precipitation at 3-hourly intervals was preprocessed to avoid an overwhelming number of extremely thin snow layers at the surface. When snowfall starts, snow is stored until there is a 12 h gap without precipitation or for a maximum of 24 h. All the snow stored during this period is then deposited in a single time step. Because snow metamorphism is a slow process at the temperatures prevailing at Dome C, this offset between snowfall and snow deposition does not impact the simulated snow profiles. All these modifications ensured that the stratification and singular physical properties of the top of the snowpack were preserved.

The simulation 1D-Ant' is similar to the simulation 1D-Ant except that the precipitation was preprocessed following the parameterization suggested by *Groot Zwaaftink et al.* [2013], that is snow was deposited only after drift events, defined as periods of 100 h with average wind at 3 m larger than 4 m s^{-1}.

3.3. Multipatch Simulations (MP, MP', and MP")

The simulation MP is based on a new parameterization, at the interface between the atmospheric forcing and the detailed snowpack model, where snow can be eroded and deposited elsewhere stochastically during drift events. Fifty parallel one-dimensional simulations were driven by the same meteorological forcing, except for the precipitation. Each simulation is referred to as a patch. The patches are not physical neighbors but an abstract representation of the spatial variability. Contrary to the explicit two-dimensional implementations of snow transport presented by, e.g., *Gallée et al.* [2001], *Lehning and Fierz* [2008], and *Vionnet et al.* [2014], here snow mass transfers do not follow any atmospheric flow, which would be difficult to model at the scales considered here [*Liston et al.*, 2007]. Nevertheless, based on the various assumptions done for the calculations, the patches must be larger than meter scale at which spatial correlation is significant (e.g., sastrugi) and smaller than the distance traveled by drifted snow during one time step of the model (900 s). A size of about 20 m × 20 m meets these constraints and is also consistent with the interspacing of the stake network and with the horizontal extent of density and SSA measurements performed for this study, to which the simulation MP is further compared. The general workflow of the parameterization of erosion and redeposition is detailed below:

1. *Detection of drift events*. Drift events are detected in the time series of ERA-Interim wind speed. A drift event starts when wind speed at 10 m exceeds 7 m s^{-1} [*Li and Pomeroy*, 1997] and is considered finished when followed by a period of 24 h with wind less than 7 m s^{-1} . *Li and Pomeroy* [1997] derived this threshold wind speed from the distribution of the threshold wind speeds, which they defined as "the wind speed when snow particles just start to move." To check this, initiation of snow transport was identified from the hourly pictures of the snow surface. The results in Figure 5 are similar to those obtained by *Li and Pomeroy* [1997], which were based on winter observations in Canada. In addition, ERA-Interim wind

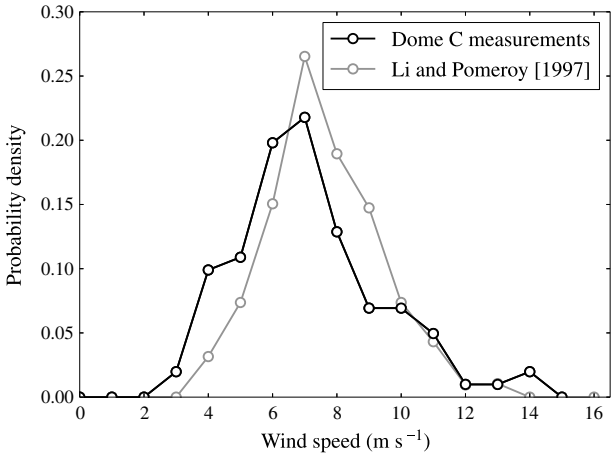

Figure 5. The dark line shows the distribution of ERA-Interim 10 m wind speed at the beginning of each of the 101 drift events identified from the pictures of surface snow (the bin size is 1 m s^{-1}). The distribution obtained by *Li and Pomeroy* [1997] for observations in Canada (their figure 2) is shown in light gray for comparison.

speed was evaluated by comparing it to wind speed records measured at 9.3 m at Dome C on an instrumented tower [*Genthon et al.*, 2013]. During the period 1st July 2011 to 1 January 2012, which did not show obvious measurement errors, no major differences were noted between both time series. They were largely correlated ($r = 0.69$) and ERA-Interim showed a positive bias of 0.21 m s^{-1}, partly explained by the height of the sensor, lower than the 10 m of ERA-Interim wind speed. The detection of drift events was applied to both time series, which led to 35 and 34 drift events for the measurements and reanalysis, respectively. This suggests that ERA-Interim reanalyses, chosen because a consistent time series of atmospheric variables on a long period was needed, are appropriate to study snow drift at Dome C.

2. *Snow erosion*. The amount of snow eroded during a drift event depends on the cohesion of surface snow and the intensity of wind. For all patches, snow layers are removed from top downwards, until a nondriftable layer or the maximum amount of erosion is reached.

    a. The driftability index, introduced by *Guyomarc'h and Mérindol* [1998] and extended to a wider density range by *Vionnet et al.* [2012], is computed for each layer at the end of a drift event using the maximum wind speed during the event.
    b. The maximum quantity of snow F that can be eroded from a patch during a time step Δt is calculated after *Naaim et al.* [1998, equation (14)]:

$$F = \Delta t \rho_a A \left(u_*^2 - u_{*t}^2\right), \tag{2}$$

where ρ_a is air density, A a coefficient depending on intergranular bonding of the snow, u_{*t} is the threshold friction velocity, and u_* is the friction velocity. According to *Naaim et al.* [1998], we chose $\rho_a A = 7 \times 10^{-4}$ kg m^{-4} s. u_{*t} and u_* are calculated after the parameterization of *Louis* [1979]:

$$u_*^2 = a^2 u_{10}^2 F_m \left(\frac{10}{z_0}, R_i\right), \tag{3}$$

where u_{10} is ERA-Interim wind speed at 10 m, a is the drag coefficient in neutral conditions, and R_i the Richardson number of the boundary layer. R_i is a diagnostic output of SURFEX/ISBA-Crocus, and the expressions for the stability function F_m in stable ($R_i > 0$) and unstable ($R_i < 0$) conditions are given in *Louis* [1979]. Here the roughness length z_0 was set to 1 mm, as in *Brun et al.* [2011] who showed that it yielded the best fit between Crocus and observed surface temperature at Dome C. This is also the value suggested by *Lenaerts et al.* [2012] and *Groot Zwaaftink et al.* [2013]. Using $z_0 = 0.1$ mm, which is of the order of the values used by *King and Anderson* [1994] and *Kuipers Munneke et al.* [2009]—0.056 mm and 0.38 mm, respectively—resulted in poorer agreement with the observed distribution of annual accumulation. It is due to the lower number of simulated drift events and smaller amount of drifted snow, which also reduced the variability in simulated SSA and density. The maximum quantity of snow removable from the snowpack during a drift event is obtained by integration along the whole event. If it is larger than 12 kg m^{-2}, the drift event is considered major and split into several consecutive events to prevent the deposition of unrealistically large layers in one step. Without this condition, layers of drifted snow thicker than 50 cm were formed, which is contradictory to observations of surface relief at Dome C [*Frezzotti et al.*, 2005].

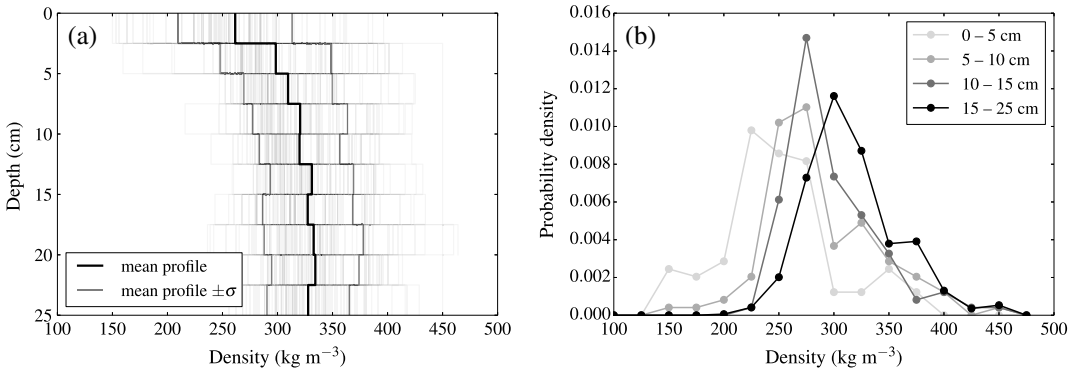

Figure 6. (a) Profiles of density of the top 25 cm of the snowpack measured during the summer campaign 2012–2013. A total of 98 profiles are shown, as well as the mean profile. The standard deviation of the measurements is also highlighted. (b) Distribution of measured densities for various depths (the bin size is 25 kg m^{-3}).

3. *Stochastic snow redeposition*. According to the observations of section2, snow is deposited on approximately 20% of the surface after a drift event. In the model, the amount of eroded snow is randomly partitioned and deposited on the 10 patches (20% of 50) with lowest snow height. Based on the observations that grains with higher SSA are preferentially found at the surface after wind events [*Kuhn et al.*, 1977; *Grenfell et al.*, 1994], drifted snow is deposited at the surface in five time steps of 15 min each, that with highest SSA deposited first and that with lowest SSA deposited last. This also prevents the formation of too thick numerical layers at the surface, that the aggregation scheme is currently unable to split instantaneously. It takes in fact several time steps to reach the optimal layer thickness from thick layers. In the meantime, the temperature profile close to the surface is poorly resolved and the metamorphism rate is incorrect. Contrary to drifted snow, precipitation is not sorted in terms of SSA, which is not critical because it corresponds to much smaller amount of snow. Since snow compaction by the wind is already accounted for by Crocus, the density of the deposited snow is equal to the average density of all eroded snow.

The simulation MP' is the same as simulation MP, except that the SSA of drifted snow was increased by 10 m^2 kg^{-1} compared to that of eroded snow. The simulation MP" is the same as simulation MP, except that the rate of increase of optical radius was divided by 2. The simulations MP, MP', and MP" were performed only with the parameterization F06.

4. Results

The simulations are now analysed by comparing the profiles of density and SSA simulated with Crocus to those measured in the field, with special attention paid to the variability.

4.1. Variability of Observed Snow Profiles

The 98 density profiles are shown in Figure 6a, along with the mean profile. The mean density increases from 260 kg m^{-3} at the surface to 330 kg m^{-3} at 25 cm which is consistent with the values reported by *Gallet et al.* [2011] and close to the average density of 280 kg m^{-3} found by *Takahashi and Kameda* [2007] for the top 10 cm of the snowpack at Dome Fuji. Density generally increases with depth as highlighted by the distributions of density at various depths (Figure 6b). The standard deviation of density decreases from 52 kg m^{-3} at the surface to 37 kg m^{-3} at 25 cm depth. The profiles are characterized by a large vertical variability, with a mean standard deviation of 39 kg m^{-3} for a single profile. This characteristics was observed similarly by *Dang et al.* [1997] who pointed out the rapid succession of layers with largely varying densities in the top meter of the snowpack at South Pole.

The 98 profiles of SSA and the mean profile are shown in Figure 7a. SSA generally decreases with depth (Figure 7b), and the mean profile decreases from approximately 50 m^2 kg^{-1} at the surface to 20 m^2 kg^{-1} at 50 cm, as found by *Gallet et al.* [2011]. This characteristic, already observed in Antarctica [*Gay et al.*, 2002] and Greenland [*Dadic et al.*, 2008], is expected because deeper snow is also older and has experienced more metamorphism and SSA decrease. The standard deviation of SSA also decreases with depth, from 35 m^2 kg^{-1} at the surface to 8 m^2 kg^{-1} at 50 cm depth.

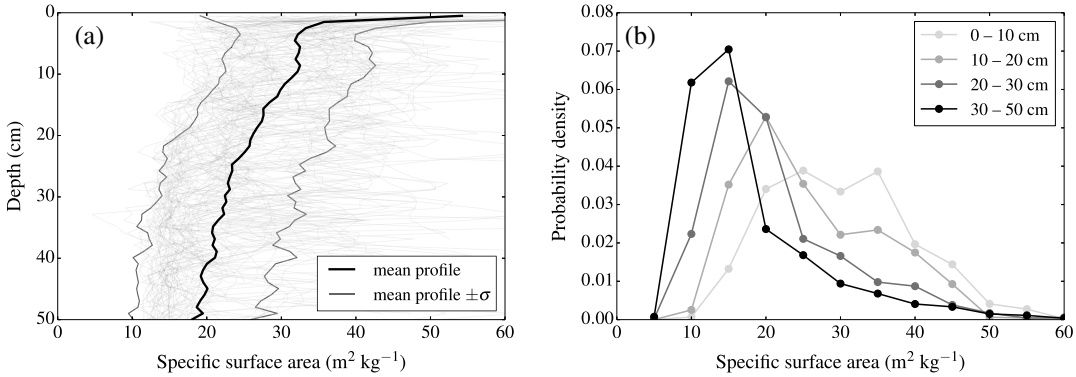

Figure 7. (a) Profiles of SSA of the top 50 cm of the snowpack measured with ASSSAP during the summer campaign 2012–2013. 98 profiles are shown, as well as the mean profile. The standard deviation is also shown. (b) Distribution of SSA for various depths (the bin size is 5 m^2 kg^{-1}).

These measurements span 2 months, so that the observed variability combines spatial and temporal variability. Both contributions were estimated from the time series of average density and SSA in the range $0-5$ cm and $20-25$ cm (Figure 8). At 25 cm depth, density does not show a temporal trend and the total variability is essentially spatial. On the contrary, the density at the top of the snowpack is more dependent on weather conditions and a slight but significant decrease of 1 kg m^{-3} d^{-1} is observed during the whole period. The large dispersion of the measurements around the trend line corresponds to spatial variability. As for SSA, it clearly decreases with time close to the surface, which is the signature of summer metamorphism [*Jin et al.*, 2008; *Kuipers Munneke et al.*, 2008; *Picard et al.*, 2012], but a large spatial variability is superimposed on this temporal trend. At greater depth, SSA shows nearly no seasonal trend and the variability is, again, essentially spatial. This reinforces the need of multipatch approaches rather than adding noise to the forcings.

4.2. One-Dimensional Simulations (1D-Std, 1D-Ant)

For the one-dimensional simulations, the simulated density and SSA profiles were averaged over the period when measurements were taken at Dome C. The average profiles obtained with the simulation 1D-Std are shown in Figure 9 along with the observations. The simulated density is lower than the observed one, in particular in the upper layers, with a mean bias of −57 kg m^{-3} for C13 and −63 kg m^{-3} for F06. SSA is also lower than the observations with mean bias of −8 m^2 kg^{-1} for both C13 and F06. These results highlight that the standard version of Crocus is not suitable for simulations of the vertical profiles of snow physical properties on the Antarctic Plateau.

The profiles obtained with the simulation 1D-Ant are shown in Figure 10. The mean density profile is much better reproduced than in simulation 1D-Std, with a mean bias of 8 kg m^{-3} for both C13 and F06 and a root mean square deviation (RMSD) of 16 kg m^{-3} for C13 and 19 kg m^{-3} for F06. The mean bias for SSA

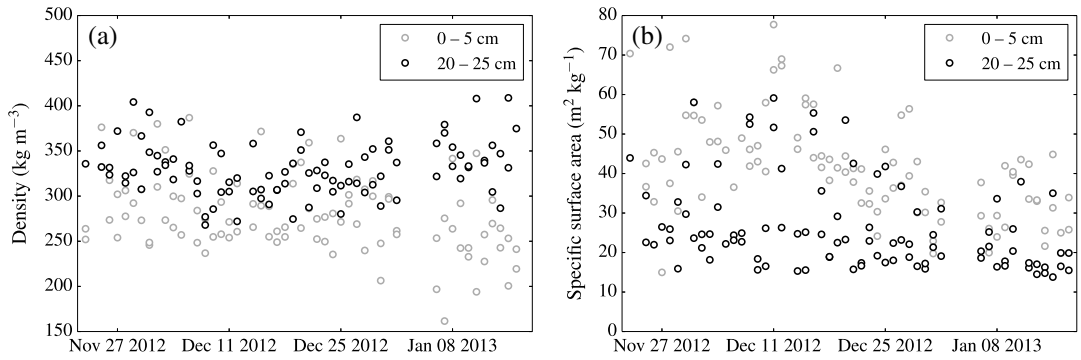

Figure 8. Time series of measured (a) density and (b) SSA (averages in the range 0–5 cm and 20–25 cm).

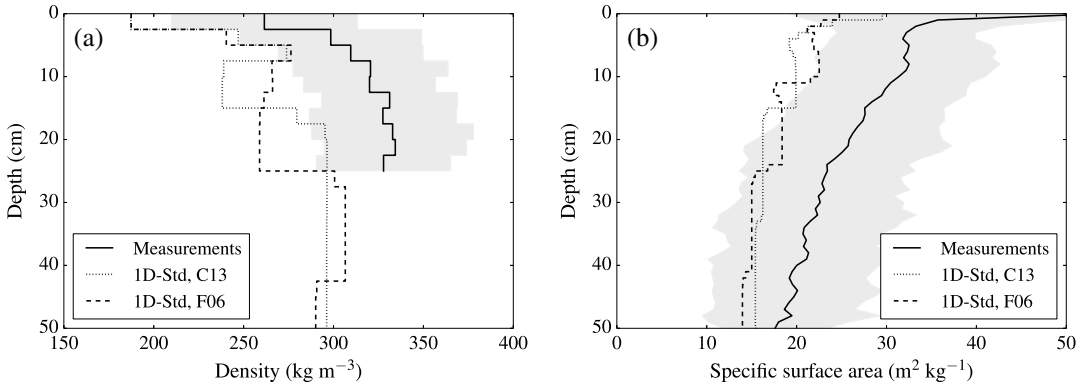

Figure 9. Average vertical profiles of (a) density and (b) SSA obtained with simulation 1D-Std on the period 23 November 2012 to 16 January 2013 and interpolated to measurements points. The average measured profiles are also shown. The shaded areas indicate the standard deviation of the measurements.

are reduced as well but remain negative, with −8 and −4 m^2 kg^{-1} for C13 and F06, respectively. The RMSD are 8 and 6 m^2 kg^{-1} for C13 and F06, respectively. SSA decreases too rapidly with depth compared to the observations but F06 performs better. The vertical profile of SSA obtained with F06 exhibits alternating layers of high and low SSA (e.g., at 20 and 22 cm) and SSA decreases down to 40 cm. This stratification is the consequence of seasonal cycles. Indeed, most of the snow metamorphism in the model occurs between late October and early March. Within this 4 month period, the layer of approximately 6 cm deposited during winter is subject to large temperature and temperature gradients, sufficient to metamorphose the whole seasonal layer into low SSA snow [*Dang et al.*, 1997]. Snow deposited at the end of summer and during fall is buried before the next summer and gives rise to the higher SSA layers. Surprisingly, the SSA profile obtained with C13 is different, without visible seasonal variations. Below 10 cm, snow has a nearly constant SSA of approximately 16 m^2 kg^{-1}. The rate of decrease near the the surface is also too rapid, which suggests that the formulation C13, based on laboratory experiments in the case of strong temperature gradients [*Marbouty*, 1980], is not appropriate for Dome C conditions. This led us to discard this formulation in favor of F06 in the following multipatch simulations. The hatched areas in Figure 10 highlight the standard deviation of the profiles simulated with F06 along the season. This represents only the temporal variability because no spatial variability can be taken into account in this simulation. Hence, the simulation greatly underestimates the variability, except for the top 2.5 cm. As for SSA, the variability in the top 8 cm is well reproduced by the simulation while below the latter shows almost no variability.

The profiles obtained with the simulation where snow is deposited only during wind events (1D-Ant') as suggested by *Groot Zwaaftink et al.* [2013] are also shown in Figure 10. The RMSD are 23 kg m^{-3} and

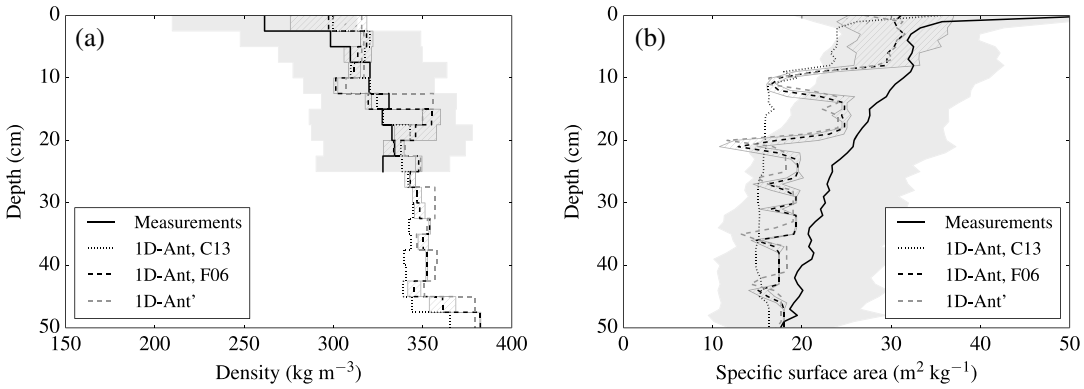

Figure 10. Average vertical profiles of (a) density and (b) SSA obtained with simulations 1D-Ant and 1D-Ant' and interpolated to measurements points. The average measured profiles are also shown. The shaded areas indicate the standard deviation of the measurements. The hatched areas indicate the standard deviation of the simulated profiles.

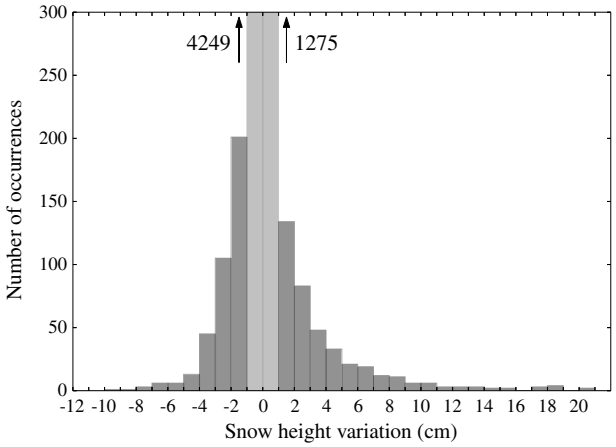

Figure 11. Distribution of snow height variations between the beginning and the end of the drift events in simulation MP.

7 m^2 kg^{-1} for the density and SSA profiles respectively. Accounting for drift events in this way did not improve the agreement between simulated and measured SSA profiles.

The version of Crocus adapted to Dome C conditions reproduced the observed density and SSA profiles better than the standard simulation in average and was used for the subsequent multipatch simulations that aim to improve the spatial variability of simulated snow properties.

4.3. Multipatch Simulations (MP)

The stochastic representation of erosion and deposition is first evaluated using in situ observations of drift events. The distribution of annual accumulation and the variability of the snow profiles obtained with the multipatch simulations are then compared to the observations.

4.3.1. Evaluation of the Snow Drift Algorithm

While 101 drift events were detected from the pictures of the snow surface, 89 were simulated in simulation MP, among which 56 are true positives (TP), 9 occurred during periods without observations, and 24 are false positives (FP). Hence, there are 45 false negatives (FN) and the precision TP/(TP+FP) of the algorithm is 0.7, while its recall TP/(TP+FN) is 0.55 [*Liang et al.*, 2012]. Given the relative simplicity of the snow drift algorithm, this is considered satisfactory. The limited accuracy of ERA-Interim wind may also contribute to this discrepancy between model and observations. Snow height variations between the beginning and the end of the events were calculated for all patches and their distribution is shown in Figure 11. Of the events, 10% resulted in net accumulation larger than 1 cm and 11% resulted in erosion larger than 1 cm. The relative proportions of erosion and deposition are thus similar to the observed proportions (Figure 2b), showing that the erosion and deposition processes were modeled adequately. However, the occurrence of net variations larger than 1 cm is less than in the observations. Simulated variations range from −10 to 21 cm, which is slightly broader than the observed range. A few events led to snow deposition larger than 15 cm, which was not observed. They are counterbalanced by erosion events less than 1 cm which are much more frequent than in the observations. In the model, each drift event leads to erosion while in the observations, erosion is a more continuous process sometimes difficult to identify in the pictures. This may explain the difference between model and observations.

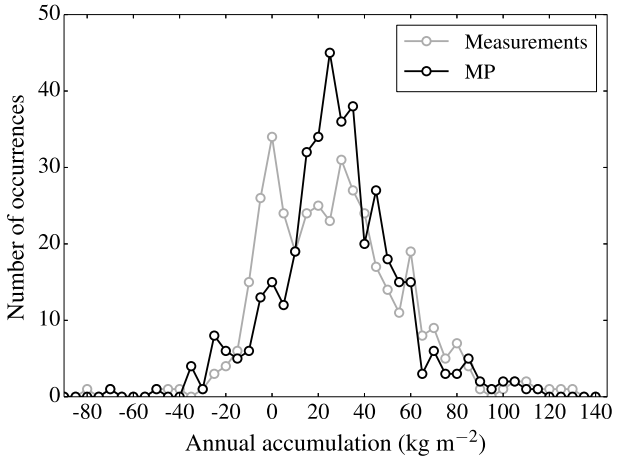

Figure 12. Distributions of annual accumulation from 2004 to 2012, measured at Dome C and obtained from simulation MP.

4.3.2. Statistics of Annual Accumulation

The annual accumulations calculated on December 1st from 2004 to 2012 for the 50 patches of simulation MP were compared to the observations (Figure 12). To this end, measured height variations were converted into accumulations, using a density value such that mean measured and simulated annual accumulations are the same. The mean simulated accumulation is 30.6 kg m^{-2} and the standard deviation is 26.3 kg m^{-2}. In the simulation, 11% of the annual accumulations are negative and 23% are lower than half the mean, which compares well with the observed 15% and 21% reported in section 2. The observed and simulated annual accumulations

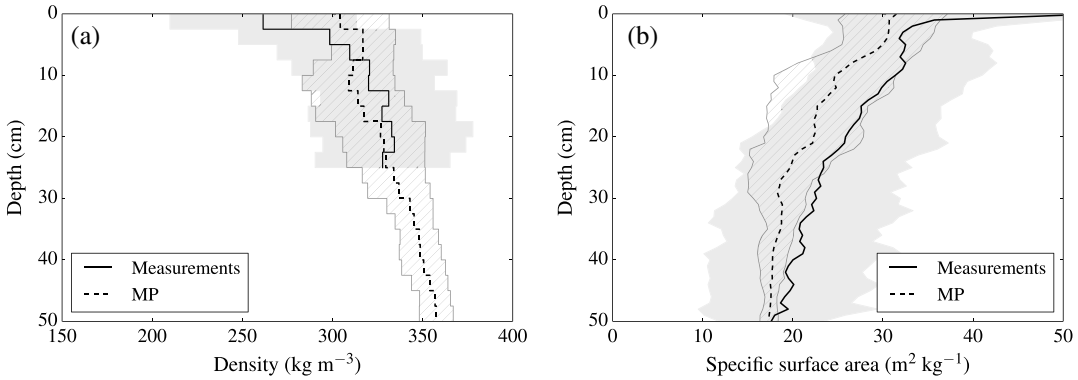

Figure 13. Vertical profiles of (a) density and (b) SSA obtained with simulation MP and interpolated to measurements points. The average measured profiles are also shown. The shaded areas indicate the standard deviation of the measurements. The hatched areas indicate the standard deviation of the simulated profiles.

range from −80 to 130 kg m^{-2} and the similarity of the distributions are very satisfactory. Annual accumulation in the simulation peaks around the mean, while the distribution of observations exhibits another peak at 0 kg m^{-2}. Despite this slight difference in the shape of the distributions, the stochastic representation of snow erosion and deposition reproduces well the variability of annual accumulation, including the years with net ablation reported by *Petit et al.* [1982], which was impossible with one-dimensional simulations.

4.3.3. Statistics of Snow Physical Properties

The density and SSA profiles obtained with simulation MP are now compared to the measured profiles. For a fair comparison and to mimic the experimental protocol, two patches (out of the 50) were chosen randomly every day from the simulation, from 23 November 2012 to 16 January 2013. The corresponding density and SSA profiles are shown in Figure 13, along with the average simulated and measured profiles.

With a mean bias of 18 kg m^{-3} and a RMSD of 28 kg m^{-3}, the average density profile of the top 25 cm is close to that obtained from all measurements and similar to that obtained in the simulation 1D-Ant. The standard deviation of the simulated density profiles is approximately 20 kg m^{-3}, which is less than the average observed standard variation of 42 kg m^{-3}. For a finer analysis, the distributions of simulated density at various depths are compared to the observations in Figure 14. These distributions are relatively similar, except for the extremes. Indeed, the low surface densities (< 200 kg m^{-3}) measured in the top 5 cm are not reproduced by the model so that for the top 10 cm, the maximum of the distribution is slightly greater in the model than in the observations. Deeper, density values larger than 375 kg m^{-3} are hardly reproduced either. This suggests that snow compaction by the wind is not adequately represented in Crocus and should be stochastically simulated to account for rare cases. These minor shortcomings explain the smaller

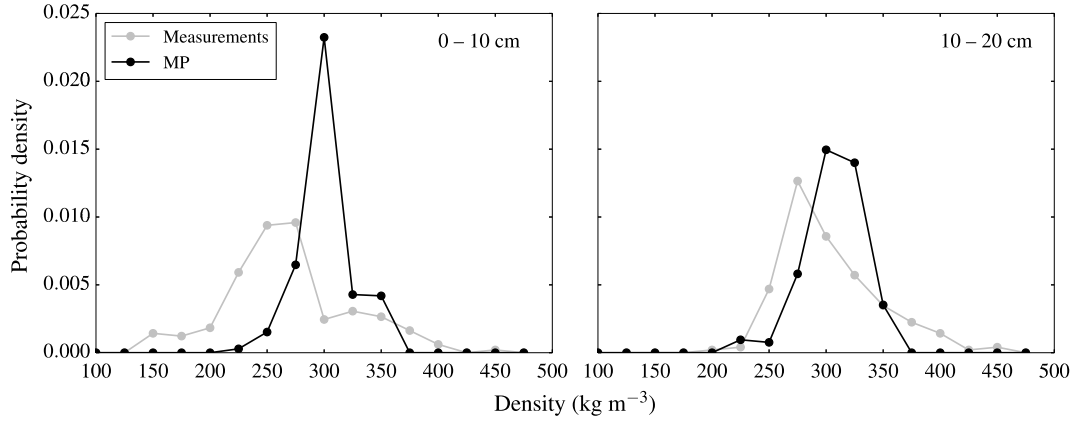

Figure 14. Distributions of measured and simulated densities at various depths for simulation MP (the bin size is 25 kg m^{-3}).

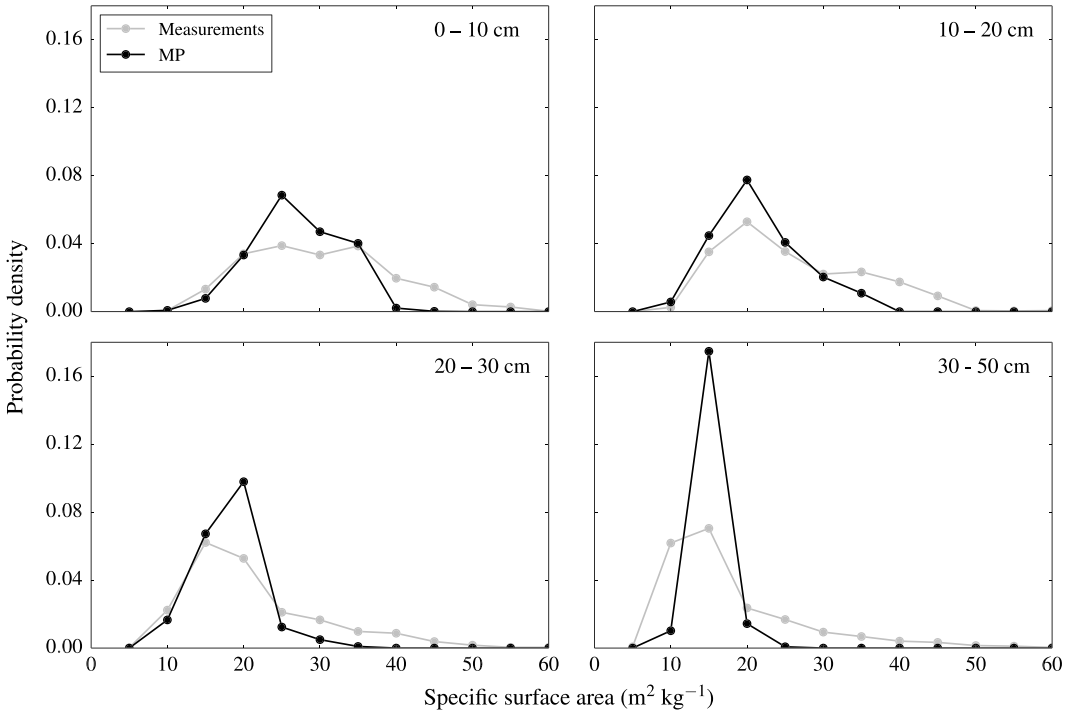

Figure 15. Distributions of measured and simulated SSA at various depths for simulation MP (the bin size is 5 m^2 kg^{-1}).

standard deviation of simulated profiles compared to the observations but the improvement with respect to simulation 1D-Ant is significant.

As for SSA, with a mean bias of −4 m^2 kg^{-1} and a RMSD of 5 m^2 kg^{-1}, the average profile of the top 50 cm still exhibits lower values than in the measurements but is improved compared to simulation 1D-Ant. The standard deviation is maximum at the surface at 5 m^2 kg^{-1} and decreases with depth down to 1 m^2 kg^{-1} at 50 cm, which is less than in the observations. The distributions of simulated SSA at various depths are compared to the observations in Figure 15. They are in general similar and the maximum of the distribution is the same in the model and in the observations, except in the range 20 – 30 cm. However, the model is unable to reproduce SSA values larger than 40 m^2 kg^{-1} at depths greater than 10 cm and underestimates the variability below 30 cm.

4.3.4. Simulations MP′ and MP″

In simulations MP′ and MP″, the SSA of drifted snow and the rate of SSA decrease, respectively, were modified with respect to simulation MP, to investigate the negative bias of the simulated SSA profiles. The SSA profiles and the distributions of SSA at various depths obtained with the simulation MP′ are shown

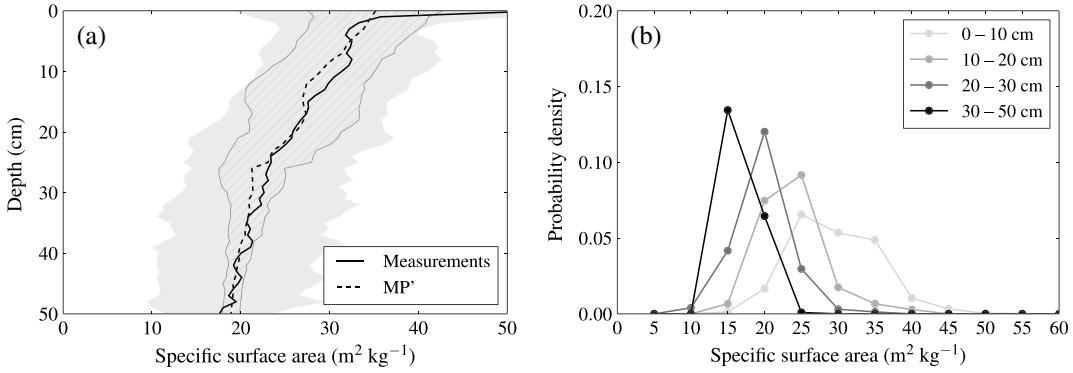

Figure 16. (a) Same as Figure 13b but for simulation MP′, i.e., increasing the SSA of drifted snow by 10 kg m^{-2}. (b) Distributions of simulated SSA at various depths (the bin size is 5 m^2 kg^{-1}).

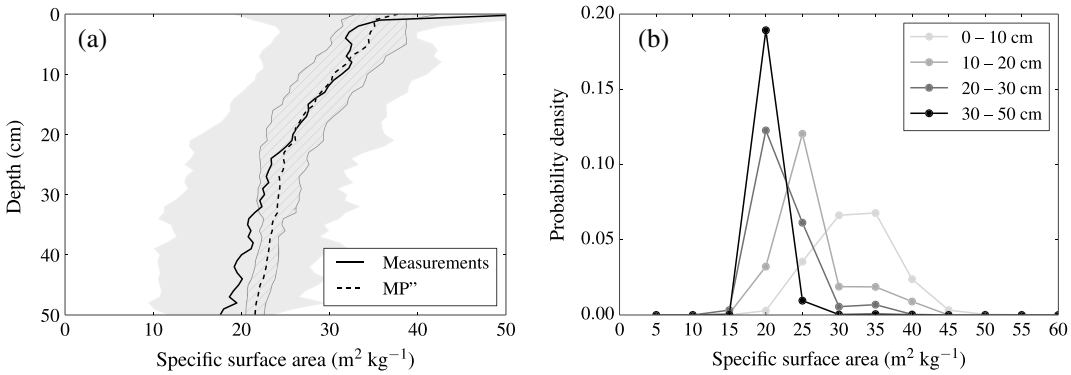

Figure 17. (a) Same as Figure 13b but for simulation MP", i.e., dividing by 2 the rate of growth of optical radius of the parameterization F06. (b) Distributions of simulated SSA at various depths (the bin size is 5 m^2 kg^{-1}).

in Figure 16. Increasing the SSA of drifted snow by 10 m^2 kg^{-1} produced a mean profile with higher SSA, thus reducing the bias to 1 m^2 kg^{-1} and the RMSD to 3 m^2 kg^{-1}. It also increased the variability of SSA at all depths, and more particularly in the top 20 cm, with the standard deviation reaching 8 m^2 kg^{-1} at the surface. Simulation MP' is thus in better agreement with the observations than simulation MP. As for simulation MP", the simulated SSA profiles and the distributions of SSA at various depths are shown in Figure 17. Dividing by two the rate of growth of optical radius produced a profile with larger SSA in good agreement with the observation, reducing the bias to 1 m^2 kg^{-1} and the RMSD to 3 m^2 kg^{-1}. However, it did not change the SSA variability at depth compared to simulation MP.

5. Discussion

From the observation of snow height variations at Dome C, we noted that snow deposition mainly occurred during drift events, as suggested by *Groot Zwaaftink et al.* [2013]. A stochastic scheme of snow erosion and deposition was thus implemented in Crocus to account for the redistribution of snow during drift events and its consequences for the internal properties of the snowpack. The ability of this parameterization to reproduce the observed snow variability is now discussed, and the current limits of the model are pointed out in the light of the simulations.

5.1. Influence of Snow Drift on Spatial Variability

The new parameterization produced variability in annual accumulation and, in turn, in snow physical properties, which was impossible with one-dimensional simulations. Despite its relative simplicity, the parameterization allowed for the first time to explain quantitatively the statistics of annual accumulation at Dome C, including the existence of local accumulation hiatus, i.e., years with net ablation, which are critical for interpretation of ice cores [*Courville et al.*, 2007]. The spatial variability of snow properties at the surface was also simulated rather successfully, with a large part of the observed variability explained by the model. This shows quantitatively the interdependence between wind, accumulation, and snow metamorphism, which was known only qualitatively [e.g., *Albert et al.*, 2004; *Hutterli et al.*, 2009]. The parameterization is built upon a limited number of parameters. Although the latter were determined from observations at Dome C, the parameterization should be suitable for a large area of the Antarctic Plateau where accumulation is low and the influence of wind on the stratification is predominant.

In fact, snow redistribution by the wind generates differences in accumulation which in turn drive differences in SSA and density as observed in the megadunes [*Courville et al.*, 2007]. Erosion and deposition impact the residence time of snow within the zone of strong temperature gradients close to the surface [*Albert et al.*, 2004; *Hutterli et al.*, 2009]. The stochastic representation of snow redeposition allows the deposition of relatively thick snow layers ($\sim$ 10–20 cm) as observed in the field, although maximum daily precipitation at Dome C in ERA-Interim during the period of simulation was less than 3 kg m^{-2}. When a layer thicker than 10 cm is deposited during a drift event, it insulates the layers below from the large temperature gradients and the penetration of solar radiation. Layers with high SSA are thus preserved deeper into the snowpack in simulation MP compared to simulation 1D-Ant (Figure 13b), in agreement with the observations of *Gay et al.* [2002] and *Gallet et al.* [2011] at Dome C. In simulation 1D-Ant, where small quantities

of snow are deposited continuously throughout the year, the annual snow layer is almost entirely metamorphosed into grains with low SSA in summer (see Figure 10b), since the simulated temperature gradients are close to 100 K m^{-1}, and exceed 300 K m^{-1} at times. This strong summer metamorphism close to the surface, that limits the advection of layers with high SSA at depth, corresponds to what *Alley et al.* [1990] observed in Greenland. Likewise, if snow remains at the surface for a long period, sometimes more than one year, it experiences intense metamorphism and is transformed into a layer with low SSA. The variability in accumulation generated by the stochastic representation thus led to variability in simulated density and SSA that was not obtained in the one-dimensional simulations.

5.2. Simulated SSA Variability

While the variability of annual accumulation is well reproduced by simulation MP (the observed and simulated standard deviations are 33 and 26 kg m^{-2}, respectively), those of SSA and density are still underestimated (mean standard deviations of 3.5 and 10 m^2 kg^{-1} for the SSA and 24 and 42 kg m^{-3} for density). The underestimation of SSA variability is partly due to the inability of the model to simulate high SSA layers at depth (see Figure 15). Indeed, the vertical variability of SSA decreases with depth due to the aggregation of numerical layers which often results in layers larger than 10 cm beyond 30 cm. The underestimation of SSA values in simulation MP is now investigated.

First, the deposition events larger than 1 cm simulated by the model are less than in the hourly observations of snow height (they represent 58% of the observed deposition events but only 21% of the simulated ones) which is explained by the absence of processes in the model to make relief features such as sastrugi [e.g., *Gow*, 1965]. In the model, only eroded snow can be randomly deposited, while our pictures of the snow surface show that snow movements are mostly due to migration of surface relief (like dune progression) rather than deposition of snow drifted from several meters at least. Large quantities of snow can thus be displaced over a short distance even with moderate winds. This process, which is not simulated by the model, may explain the differences between observed and simulated snow height variations during drift events. As a consequence, the differences in accumulation and the insulating effect of drifted snow are probably smaller in the model than in reality.

Second, the SSA of drifted snow in simulation MP is assumed equal to that of eroded snow although former studies suggest that snow drift results in higher SSA due to sublimation and breaking of the grains [e.g., *Domine et al.*, 2009]. The impact of such an increase of SSA during drift events was estimated with simulation MP′, in which the SSA of drifted snow was increased by 10 m^2 kg^{-1} compared to that of eroded snow. This resulted in a large improvement, with average SSA profile very close to the mean observed profile, highlighting that small changes in SSA at the surface are propagated deep into the snowpack. The increase of SSA during drift events may thus explain all the negative bias obtained in simulation MP where this process was not accounted for. The standard deviation of SSA was also increased at all depths and in particular in the top 5 cm (where it increased from 5 m^2 kg^{-1} in simulation MP to 6.5 m^2 kg^{-1} in simulation MP′) because in simulation MP′ the snow surface is regularly refreshed with high SSA grains.

The underestimation of SSA in simulation MP compared to observations may also be due to the parameterization of snow metamorphism. Indeed, the simulation 1D-Ant showed that the SSA profile was sensitive to the parameterization of metamorphism (Figure 10b). The presence of snow all year long implies that metamorphism operates on long time scales compared to alpine snow for which the parameterizations were developed. For instance, the parameterization F06 is based on a fit of the full model of *Flanner and Zender* [2006] on 14 days even at low temperatures where metamorphism is known to be very slow. The sensitivity of the profiles to the parameterization F06 was estimated by dividing by two the rate of growth of optical radius (simulation MP″). This improved the overall match between average simulated and measured SSA profiles but produced too high SSA at depth and did not increase the simulated variability (Figure 17). Indeed, the parameterization F06 leads to nearly constant SSA at the time scale of a few years so that SSA singularities are not conserved on the long term. This is one of the reasons why SSA variability at depth is too weak in the simulations.

5.3. Modeling the Very Dense Layers

In terms of density, no simulation reproduces the extreme values and in particular the low values observed at the surface (Figure 14). In a simulation similar to 1D-Ant, the density of fresh snow was set to 50 kg m^{-3} instead of 170 kg m^{-3} to estimate the impact on the density profile. This reduced the bias in the top 2.5 cm from 40 kg m^{-3} (simulation 1D-Ant) to 10 kg m^{-3}, but did not change significantly the density deeper. It also

produced SSA profiles with values approximately 5 m^2 kg^{-1} lower than in 1D-Ant, since temperature gradient metamorphism was amplified at low density [*Flanner and Zender*, 2006]. Most measured densities lower than 200 kg m^{-3} were obtained when layers of wind blown surface hoar thicker than 2 cm were present at the surface. The formation of surface hoar, characterized by low density, is poorly known [*Gow*, 1965; *Champollion et al.*, 2013] and is not reproduced by the model although it may have a large impact on surface snow density [*Lacroix et al.*, 2009; *Brucker et al.*, 2014]. Regarding layers with high density, the stochastic approach enables layers with densities up to 350 kg m^{-3} to form when they remain at the surface for long periods, but it rarely yields density values larger than 375 kg m^{-3}, although such hard layers can form at the surface and are preserved at depth (Figure 6b). These surface layers with density as high as 475 kg m^{-3} are typical features of the Antarctic Plateau [*Albert et al.*, 2004; *Scambos et al.*, 2012; *Picard et al.*, 2014], but the processes of their formation are not entirely understood [*Kameda et al.*, 2008] and not taken into account in the model. The parameterization of post-depositional snow compaction by the wind implemented in Crocus was initially adjusted to match temperature profiles at South Pole. It is thus not physically based and was not derived from direct measurements of snow compaction which may limit its application.

6. Conclusions

In the light of in situ observations of snow height variations, a new parameterization of snow erosion and deposition by the wind was implemented in the model Crocus to better capture the observed spatial variability of annual accumulation, density, and SSA at Dome C. This parameterization followed a stochastic approach by allowing mass transfers among a set of 50 patches during strong wind events. This model simulated successfully the statistics of annual accumulation at Dome C (including the years with net ablation), whose variability drives the variability of snow physical properties. The simulated density and SSA profiles obtained with this parameterization were compared to an extended set of 98 shallow snow profiles taken during the summer 2012–2013. The observed variability of snow properties at the surface were well reproduced, which highlighted the crucial role of wind as a driver of surface snow properties, even at Dome C where winds are generally weak. However, singular features such as layers with density larger than 375 kg m^{-3} near the surface and layers with SSA larger than 40 m^2 kg^{-1} at depth remain out of reach of the model, emphasizing the need to better understand the physical processes operating close to the surface. In particular, the sastrugi are not represented in the model, although they influence local accumulation and erosion [*Gow*, 1965], surface roughness [*Champollion et al.*, 2013], and snow albedo [*Wang and Zender*, 2011]. Resolving sastrugi at the meter scale using a three-dimensional physically based model for snow transport by the wind would yield a more realistic representation of the snow surface. The presence of sastrugi would indeed result in spatial variability of surface wind, allowing snow transport. Such a model might help to understand the occurrence and intensity of drift events and the consequent snow height variations, as well as the formation of extremely dense snow layers. This would be however computationally too expensive for climate studies. Despite its current limits, the suggested parameterization is already promising for extended studies of surface snow evolution and surface mass balance on the Antarctic Plateau. It is also of interest for paleoclimatology studies and remote sensing applications for which the variability of snow physical properties is a large source of uncertainty.

Acknowledgments

The authors wish to thank W. Colgan and two anonymous referees for their very useful suggestions and comments. LGGE and CNRM-GAME/CEN are part of LabEx OSUG@2020 (ANR10 LABX56). This study was supported by the ANR program 1-JS56-005-01-11JS56-005-01 MONISNOW. We are grateful to the French Polar Institute (IPEV) for the logistic support at Concordia station in Antarctica through the CALVA-Neige programme and to the GLACIOCLIM-SAMBA observatory which is supported by the French and Italian (PNRA) Polar Intitutes, and the Institut National des Sciences de l'Univers (INSU). We are grateful to Matthieu Lafaysse for helpful discussions about Crocus and to Vincent Vionnet for his suggestions regarding the representation of snow transport by the wind. We thank Sophie Tyteca for providing the processed ERA-Interim forcings at Dome C. Christophe Genthon and Hélène Barral are also thanked for making available the wind speed measurements at Dome C. Olivier Saint-Jean participated in the analysis of the pictures of the snow surface. These pictures are freely available from http://www-lgge.obs.ujf-grenoble.fr/~picard/pauto/. The density and SSA measurements are available upon request from the authors.

References

Albert, M., C. Shuman, Z. Courville, R. Bauer, M. Fahnestock, and T. Scambos (2004), Extreme firn metamorphism: Impact of decades of vapor transport on near-surface firn at a low-accumulation glazed site on the East Antarctic plateau, *Ann. Glaciol.*, *39*(1), 73–78, doi:10.3189/172756404781814041.

Albert, M. R. (2002), Effects of snow and firn ventilation on sublimation rates, *Ann. Glaciol.*, *35*(1), 52–56.

Alley, R. B. (1988), Concerning the deposition and diagenesis of strata in polar firn, *J. Glaciol.*, *34*, 283–290.

Alley, R. B., E. S. Saltzman, K. M. Cuffey, and J. J. Fitzpatrick (1990), Summertime formation of depth hoar in central Greenland, *Geophys. Res. Lett.*, *17*(13), 2393–2396, doi:10.1029/GL017i013p02393.

Arnaud, L., G. Picard, N. Champollion, F. Domine, J. Gallet, E. Lefebvre, M. Fily, and J. Barnola (2011), Measurement of vertical profiles of snow specific surface area with a 1 cm resolution using infrared reflectance: Instrument description and validation, *J. Glaciol.*, *57*(201), 17–29, doi:10.3189/002214311795306664.

Arthern, R. J., D. P. Winebrenner, and D. G. Vaughan (2006), Antarctic snow accumulation mapped using polarization of 4.3-cm wavelength microwave emission, *J. Geophys. Res.*, *111*, D06107, doi:10.1029/2004JD005667.

Bromwich, D. H., J. P. Nicolas, and A. J. Monaghan (2011), An assessment of precipitation changes over Antarctica and the southern ocean since 1989 in contemporary global reanalyses, *J. Clim.*, *24*(16), 4189–4209, doi:10.1175/2011JCLI4074.1.

Brucker, L., E. P. Dinnat, G. Picard, and N. Champollion (2014), Effect of snow surface metamorphism on Aquarius L-band radiometer observations at Dome C, Antarctica, *IEEE Trans. Geosci. Remote Sens.*, *52*(11), 7408–7417, doi:10.1109/TGRS.2014.2312102.

Brun, E., E. Martin, V. Simon, C. Gendre, and C. Coléou (1989), An energy and mass model of snow cover suitable for operational avalanche forecasting, *J. Glaciol.*, *35*, 333–342.

Brun, E., P. David, M. Sudul, and G. Brunot (1992), A numerical model to simulate snow-cover stratigraphy for operational avalanche forecasting, *J. Glaciol.*, *38*, 13–22.
Brun, E., E. Martin, and V. Spiridonov (1997), Coupling a multi-layered snow model with a GCM, *Ann. Glaciol.*, *25*, 66–72.
Brun, E., et al. (2011), Snow/atmosphere coupled simulation at Dome C, Antarctica, *J. Glaciol.*, *57*(204), 721–736, doi:10.3189/002214311797409794.
Brun, E., V. Vionnet, A. Boone, B. Decharme, Y. Peings, R. Valette, F. Karbou, and S. Morin (2013), Simulation of northern Eurasian local snow depth, mass, and density using a detailed snowpack model and meteorological reanalyses, *J. Hydrometeorol.*, *14*(1), 203–219, doi:10.1175/JHM-D-12-012.1.
Carmagnola, C. M., S. Morin, M. Lafaysse, F. Domine, B. Lesaffre, Y. Lejeune, G. Picard, and L. Arnaud (2014), Implementation and evaluation of prognostic representations of the optical diameter of snow in the SURFEX/ISBA-Crocus detailed snowpack model, *Cryosphere*, *8*(2), 417–437, doi:10.5194/tc-8-417-2014.
Champollion, N., G. Picard, L. Arnaud, E. Lefebvre, and M. Fily (2013), Hoar crystal development and disappearance at Dome C, Antarctica: Observation by near-infrared photography and passive microwave satellite, *Cryosphere*, *7*(4), 1247–1262, doi:10.5194/tc-7-1247-2013.
Colbeck, S. (1989), Snow-crystal growth with varying surface temperatures and radiation penetration, *J. Glaciol.*, *35*(119), 23–29, doi:10.3189/002214389793701536.
Courville, Z. R., M. R. Albert, M. A. Fahnestock, L. M. Cathles, and C. A. Shuman (2007), Impacts of an accumulation hiatus on the physical properties of firn at a low-accumulation polar site, *J. Geophys. Res.*, *112*, F02030, doi:10.1029/2005JF000429.
Dadic, R., M. Schneebeli, M. Lehning, M. A. Hutterli, and A. Ohmura (2008), Impact of the microstructure of snow on its temperature: A model validation with measurements from Summit, Greenland, *J. Geophys. Res.*, *113*, D14303, doi:10.1029/2007JD009562.
Dang, H., C. Genthon, and E. Martin (1997), Numerical modeling of snow cover over polar ice sheets, *Ann. Glaciol.*, *25*, 170–176.
Das, I., et al. (2013), Influence of persistent wind scour on the surface mass balance of Antarctica, *Nat. Geosci.*, *6*(5), 367–371, doi:10.1038/ngeo1766.
Dee, D. P., et al. (2011), The ERA-interim reanalysis: Configuration and performance of the data assimilation system, *Q. J. R. Meteorol. Soc.*, *137*(656), 553–597, doi:10.1002/qj.828.
Domine, F., M. Albert, T. Huthwelker, H.-W. Jacobi, A. A. Kokhanovsky, M. Lehning, G. Picard, and W. R. Simpson (2008), Snow physics as relevant to snow photochemistry, *Atmos. Chem. Phys.*, *8*, 171–208.
Domine, F., A.-S. Taillandier, A. Cabanes, T. A. Douglas, and M. Sturm (2009), Three examples where the specific surface area of snow increased over time, *Cryosphere*, *3*(1), 31–39, doi:10.5194/tc-3-31-2009.
Eisen, O., et al. (2008), Ground-based measurements of spatial and temporal variability of snow accumulation in East Antarctica, *Rev. Geophys.*, *46*, RG2001, doi:10.1029/2006RG000218.
Fisher, D. A., N. Reeh, and H. B. Clausen (1985), Stratigraphic noise in time series derived from ice cores, *Ann. Glaciol.*, *7*, 76–83.
Flanner, M. G., and C. S. Zender (2006), Linking snowpack microphysics and albedo evolution, *J. Geophys. Res.*, *111*, D12208, doi:10.1029/2005JD006834.
Fréville, H., E. Brun, G. Picard, N. Tatarinova, L. Arnaud, C. Lanconelli, C. Reijmer, and M. van den Broeke (2014), Using MODIS land surface temperatures and the Crocus snow model to understand the warm bias of ERA-interim reanalyses at the surface in Antarctica, *Cryosphere*, *8*(4), 1361–1373, doi:10.5194/tc-8-1361-2014.
Frezzotti, M., et al. (2004), New estimations of precipitation and surface sublimation in East Antarctica from snow accumulation measurements, *Clim. Dyn.*, *23*(7-8), 803–813, doi:10.1007/s00382-004-0462-5.
Frezzotti, M., et al. (2005), Spatial and temporal variability of snow accumulation in East Antarctica from traverse data, *J. Glaciol.*, *51*(172), 113–124, doi:10.3189/172756505781829502.
Fujita, K., and O. Abe (2006), Stable isotopes in daily precipitation at Dome Fuji, East Antarctica, *Geophys. Res. Lett.*, *33*, L18503, doi:10.1029/2006GL026936.
Fujita, S., J. Okuyama, A. Hori, and T. Hondoh (2009), Metamorphism of stratified firn at Dome Fuji, Antarctica: A mechanism for local insolation modulation of gas transport conditions during bubble close off, *J. Geophys. Res.*, *114*, F03023, doi:10.1029/2008JF001143.
Gallée, H., G. Guyomarc'h, and E. Brun (2001), Impact of snow drift on the Antarctic ice sheet surface mass balance: Possible sensitivity to snow-surface properties, *Boundary Layer Meteorol.*, *99*(1), 1–19.
Gallet, J.-C., F. Domine, L. Arnaud, G. Picard, and J. Savarino (2011), Vertical profile of the specific surface area and density of the snow at Dome C and on a transect to Dumont D'Urville, Antarctica—Albedo calculations and comparison to remote sensing products, *Cryosphere*, *5*(3), 631–649, doi:10.5194/tc-5-631-2011.
Gay, M., M. Fily, C. Genthon, M. Frezzotti, H. Oerter, and J.-G. Winther (2002), Snow grain-size measurements in Antarctica, *J. Glaciol.*, *48*(163), 527–535, doi:10.3189/172756502781831016.
Genthon, C., D. Six, H. Gallée, P. Grigioni, and A. Pellegrini (2013), Two years of atmospheric boundary layer observations on a 45-m tower at Dome C on the Antarctic plateau, *J. Geophys. Res. Atmos.*, *118*(8), 3218–3232, doi:10.1002/jgrd.50128.
Goodwin, I. D. (1990), Snow accumulation and surface topography in the katabatic zone of Eastern Wilkes Land, Antarctica, *Antarct. Sci.*, *2*(03), 235–242.
Gow, A. J. (1965), On the accumulation and seasonal stratification of snow at the South Pole, *J. Glaciol.*, *5*(40), 467–477.
Grenfell, T. C., S. G. Warren, and P. C. Mullen (1994), Reflection of solar radiation by the Antarctic snow surface at ultraviolet, visible, and near-infrared wavelengths, *J. Geophys. Res.*, *99*, 18,669–18,684, doi:10.1029/94JD01484.
Groot Zwaaftink, C. D., A. Cagnati, A. Crepaz, C. Fierz, G. Macelloni, M. Valt, and M. Lehning (2013), Event-driven deposition of snow on the Antarctic Plateau: Analyzing field measurements with SNOWPACK, *Cryosphere*, *7*(1), 333–347, doi:10.5194/tc-7-333-2013.
Guyomarc'h, G., and L. Mérindol (1998), Validation of an application for forecasting blowing snow, *Ann. Glaciol.*, *26*, 138–143.
Hall, A. (2004), The role of surface albedo feedback in climate, *J. Clim.*, *17*, 1550–1568, doi:10.1175/1520-0442(2004)017<1550:TROSAF>2.0.CO;2.
Hansen, J. (2004), Soot climate forcing via snow and ice albedos, *Proc. Natl. Acad. Sci. U.S.A.*, *101*(2), 423–428, doi:10.1073/pnas.2237157100.
Hutterli, M. A., M. Schneebeli, J. Freitag, J. Kipfstuhl, and R. Röthlisberger (2009), Impact of local insolation on snow metamorphism and ice core records, *Low Temp. Sci.*, *68*(Supplement), 223–232.
Jin, Z., T. P. Charlock, P. Yang, Y. Xie, and W. Miller (2008), Snow optical properties for different particle shapes with application to snow grain size retrieval and MODIS/CERES radiance comparison over Antarctica, *Remote Sens. Environ.*, *112*(9), 3563–3581, doi:10.1016/j.rse.2008.04.011.
Kameda, T., H. Motoyama, S. Fujita, and S. Takahashi (2008), Temporal and spatial variability of surface mass balance at Dome Fuji, East Antarctica, by the stake method from 1995 to 2006, *J. Glaciol.*, *54*(184), 107–116, doi:10.3189/002214308784409062.

King, J., and P. Anderson (1994), Heat and water vapour fluxes and scalar roughness lengths over an Antarctic ice shelf, *Boundary Layer Meteorol.*, *69*(1-2), 101–121, doi:10.1007/BF00713297.

Koerner, R. M. (1971), A stratigraphic method of determining the snow accumulation rate at Plateau station, Antarctica, and application to South Pole-Queen Maud Land Traverse 2, 1965–1966, in *Antarctic Snow and Ice Studies II*, vol. 16, edited by A. P. Crary, pp. 225–238, AGU, Washington, D. C.

Krinner, G., O. Magand, I. Simmonds, C. Genthon, and J. L. Dufresne (2007), Simulated Antarctic precipitation and surface mass balance at the end of the twentieth and twenty-first centuries, *Clim. Dyn.*, *28*(2-3), 215–230, doi:10.1007/s00382-006-0177-x.

Kuhn, M., L. S. Kundla, and L. A. Stroschein (1977), The radiation budget at Plateau Station, Antarctica, 1966–1967, in *Meteorological Studies at Plateau Station, Antarctica, Antarct. Res. Ser.*, vol. 25, edited by A. J. Riordan et al., pp. 41–73, AGU, Washington, D. C.

Kuipers Munneke, P., C. H. Reijmer, M. R. van den Broeke, G. König-Langlo, P. Stammes, and W. H. Knap (2008), Analysis of clear-sky Antarctic snow albedo using observations and radiative transfer modeling, *J. Geophys. Res.*, *113*, D17118, doi:10.1029/2007JD009653.

Kuipers Munneke, P., M. R. van den Broeke, C. H. Reijmer, M. M. Helsen, W. Boot, M. Schneebeli, and K. Steffen (2009), The role of radiation penetration in the energy budget of the snowpack at Summit, Greenland, *Cryosphere*, *3*(2), 155–165.

Lacroix, P., B. Legresy, F. Remy, F. Blarel, G. Picard, and L. Brucker (2009), Rapid change of snow surface properties at Vostok, East Antarctica, revealed by altimetry and radiometry, *Remote Sens. Environ.*, *113*(12), 2633–2641, doi:10.1016/j.rse.2009.07.019.

Lehning, M., and C. Fierz (2008), Assessment of snow transport in avalanche terrain, *Cold Reg. Sci. Technol.*, *51*(2-3), 240–252, doi:10.1016/j.coldregions.2007.05.012.

Lehning, M., P. Bartelt, B. Brown, C. Fierz, and P. Satyawali (2002), A physical SNOWPACK model for the Swiss avalanche warning: Part II. Snow microstructure, *Cold Reg. Sci. Technol.*, *35*(3), 147–167, doi:10.1016/S0165-232X(02)00073-3.

Lenaerts, J. T. M., M. R. van den Broeke, S. J. Déry, E. van Meijgaard, W. J. van de Berg, S. P. Palm, and J. Sanz Rodrigo (2012), Modeling drifting snow in Antarctica with a regional climate model: 1. Methods and model evaluation, *J. Geophys. Res.*, *117*, D05108, doi:10.1029/2011JD016145.

Li, L., and J. W. Pomeroy (1997), Estimates of threshold wind speeds for snow transport using meteorological data, *J. Appl. Meteorol.*, *36*(3), 205–213, doi:10.1175/1520-0450(1997)036<0205:EOTWSF>2.0.CO;2.

Liang, Y.-L., W. Colgan, Q. Lv, K. Steffen, W. Abdalati, J. Stroeve, D. Gallaher, and N. Bayou (2012), A decadal investigation of supraglacial lakes in West Greenland using a fully automatic detection and tracking algorithm, *Remote Sens. Environ.*, *123*, 127–138.

Liston, G. E., R. B. Haehnel, M. Sturm, C. A. Hiemstra, S. Berezovskaya, and R. D. Tabler (2007), Simulating complex snow distributions in windy environments using SnowTran-3D, *J. Glaciol.*, *53*(181), 241–256, doi:10.3189/172756507782202865.

Louis, J.-F. (1979), A parametric model of vertical eddy fluxes in the atmosphere, *Boundary Layer Meteorol.*, *17*(2), 187–202, doi:10.1007/BF00117978.

Marbouty, D. (1980), An experimental study of temperature-gradient metamorphism, *J. Glaciol.*, *26*, 303–312.

Mott, R., and M. Lehning (2010), Meteorological modeling of very high-resolution wind fields and snow deposition for mountains, *J. Hydrometeorol.*, *11*(4), 934–949, doi:10.1175/2010JHM1216.1.

Naaim, M., F. N. Naaim-Bouvet, and H. Martinez (1998), Numerical simulation of drifting snow: Erosion and deposition models, *Ann. Glaciol.*, *26*, 191–196.

Oleson, K. W., et al. (2010), Technical description of version 4.0 of the Community Land Model (CLM), *Tech. Rep. NCAR/TN-478+STR*, Natl. Cent. for Atmos. Res., Boulder, Colo.

Palais, J. M., I. M. Whillans, and C. Bull (1983), Snow stratigraphic studies at Dome C, East Antarctica: An investigation of depositional and diagenetic processes, *Ann. Glaciol.*, *3*, 239–242.

Palerme, C., J. E. Kay, C. Genthon, T. L'Ecuyer, N. B. Wood, and C. Claud (2014), How much snow falls on the Antarctic ice sheet?, *Cryosphere*, *8*(4), 1577–1587, doi:10.5194/tc-8-1577-2014.

Petit, J. R., J. Jouzel, M. Pourchet, and L. Merlivat (1982), A detailed study of snow accumulation and stable isotope content in Dome C (Antarctica), *J. Geophys. Res.*, *87*(C6), 4301, doi:10.1029/JC087iC06p04301.

Picard, G., F. Domine, G. Krinner, L. Arnaud, and E. Lefebvre (2012), Inhibition of the positive snow-albedo feedback by precipitation in interior Antarctica, *Nat. Clim. Change*, *2*(11), 795–798, doi:10.1038/nclimate1590.

Picard, G., A. Royer, L. Arnaud, and M. Fily (2014), Influence of meter-scale wind-formed features on the variability of the microwave brightness temperature around Dome C in Antarctica, *Cryosphere*, *8*(3), 1105–1119, doi:10.5194/tc-8-1105-2014.

Raynaud, D., V. Lipenkov, B. Lemieux-Dudon, P. Duval, M.-F. Loutre, and N. Lhomme (2007), The local insolation signature of air content in Antarctic ice. A new step toward an absolute dating of ice records, *Earth Planet. Sci. Lett.*, *261*(3-4), 337–349, doi:10.1016/j.epsl.2007.06.025.

Scambos, T., T. Haran, M. Fahnestock, T. Painter, and J. Bohlander (2007), MODIS-based mosaic of Antarctica (MOA) data sets: Continent-wide surface morphology and snow grain size, *Remote Sens. Environ.*, *111*(2-3), 242–257, doi:10.1016/j.rse.2006.12.020.

Scambos, T., et al. (2012), Extent of low-accumulation "wind glaze" areas on the East Antarctic plateau: Implications for continental ice mass balance, *J. Glaciol.*, *58*(210), 633–647, doi:10.3189/2012JoG11J232.

Shepherd, A., and D. Wingham (2007), Recent sea-level contributions of the Antarctic and Greenland ice sheets, *Science*, *315*(5818), 1529–1532, doi:10.1126/science.1136776.

Steen-Larsen, H. C., et al. (2011), Understanding the climatic signal in the water stable isotope records from the NEEM shallow firn/ice cores in northwest Greenland, *J. Geophys. Res.*, *116*, D06108, doi:10.1029/2010JD014311.

Sturm, M., and C. S. Benson (1997), Vapor transport, grain growth and depth-hoar development in the subarctic snow, *J. Glaciol.*, *43*(143), 42–59.

Sugiyama, S., H. Enomoto, S. Fujita, K. Fukui, F. Nakazawa, P. Holmlund, and S. Surdyk (2012), Snow density along the route traversed by the Japanese-Swedish Antarctic Expedition 2007/08, *J. Glaciol.*, *58*(209), 529–539, doi:10.3189/2012JoG11J201.

Svensson, A., et al. (2008), A 60 000 year Greenland stratigraphic ice core chronology, *Clim. Past*, *4*(1), 47–57, doi:10.5194/cp-4-47-2008.

Taillandier, A.-S., F. Domine, W. R. Simpson, M. Sturm, and T. A. Douglas (2007), Rate of decrease of the specific surface area of dry snow: Isothermal and temperature gradient conditions, *J. Geophys. Res.*, *112*, F03003, doi:10.1029/2006JF000514.

Takahashi, S., and T. Kameda (2007), Snow density for measuring surface mass balance using the stake method, *J. Glaciol.*, *53*(183), 677–680, doi:10.3189/002214307784409360.

van de Berg, W. J., M. R. van den Broeke, C. H. Reijmer, and E. van Meijgaard (2006), Reassessment of the Antarctic surface mass balance using calibrated output of a regional atmospheric climate model, *J. Geophys. Res.*, *111*, D11104, doi:10.1029/2005JD006495.

Vionnet, V., E. Brun, S. Morin, A. Boone, S. Faroux, P. Le Moigne, E. Martin, and J.-M. Willemet (2012), The detailed snowpack scheme Crocus and its implementation in SURFEX v7.2, *Geosci. Model Dev.*, *5*(3), 773–791, doi:10.5194/gmd-5-773-2012.

Vionnet, V., E. Martin, V. Masson, G. Guyomarc'h, F. Naaim-Bouvet, A. Prokop, Y. Durand, and C. Lac (2014), Simulation of wind-induced snow transport and sublimation in alpine terrain using a fully coupled snowpack/atmosphere model, *Cryosphere*, *8*(2), 395–415, doi:10.5194/tc-8-395-2014.

Walden, V. P., S. G. Warren, and E. Tuttle (2003), Atmospheric ice crystals over the Antarctic plateau in winter, *J. Appl. Meteorol.*, *42*(10), 1391–1405, doi:10.1175/1520-0450(2003)042<1391:AICOTA>2.0.CO;2.

Wang, X., and C. S. Zender (2011), Arctic and Antarctic diurnal and seasonal variations of snow albedo from multiyear Baseline Surface Radiation Network measurements, *J. Geophys. Res.*, *116*, F03008, doi:10.1029/2010JF001864.